THE JOURNAL OF BIOLOGICAL CHEMISTRY
Vol. 273, No. 4, Issue of January 23, pp. 2153–2160, 1998

Printed in U.S.A.

High Resolution Crystal Structure of a Human Tumor Necrosis Factor-α Mutant with Low Systemic Toxicity*

(Received for publication, September 3, 1997, and in revised form, October 21, 1997)

Sun-Shin Cha‡, Jeong-Sun Kim‡, Hyun-Soo Cho‡, Nam-Kyu Shin§, Woojin Jeong§, Hang-Cheol Shin§, Yeoun Jin Kim¶, Jong Hoon Hahn¶, Byung-Ha Oh‡‖

From the ‡Department of Life Science and School of Environmental Engineering and the ¶Center for Biofunctional Molecules and Department of Chemistry, Pohang University of Science and Technology, Hyoja-dong, San 31, Pohang, Kyungbuk, 790-784, South Korea and the §Protein Engineering Laboratory, Hanhyo Institute of Technology, 461-6 Jeonmin-dong, Yusung-gu, Taejon 305-390, South Korea

A human tumor necrosis factor-α (TNF-α) mutant (M3S) with low systemic toxicity *in vivo* was designed, and its structures in two different crystal packings were determined crystallographically at 1.8 and 2.15-Å resolution, respectively, to explain altered biological activities of the mutant. M3S contains four changes: a hydrophilic substitution of L29S, two hydrophobic substitutions of S52I and Y56F, and a deletion of the N-terminal seven amino acids that is disordered in the structure of wild-type TNF-α. Compared with wild-type TNF-α, it exhibits 11- and 71-fold lower binding affinities for the human TNF-R55 and TNF-R75 receptors, respectively, and *in vitro* cytotoxic effect and *in vivo* systemic toxicity of M3S are 20 and 10 times lower, respectively. However, in a transplanted solid tumor mouse model, M3S suppresses tumor growth more efficiently than wild-type TNF-α. M3S is highly resistant to proteolysis by trypsin, and it exhibits increased thermal stability and a prolonged half-life *in vivo*. The L29S mutation causes substantial restructuring of the loop containing residues 29–36 into a rigid segment as a consequence of induced formation of intra- and intersubunit interactions, explaining the altered receptor binding affinity and thermal stability. A mass spectrometric analysis identified major proteolytic cleavage sites located on this loop, and thus the increased resistance of M3S to the proteolysis is consistent with the increased rigidity of the loop. The S52I and Y56F mutations do not induce a noticeable conformational change. The side chain of Phe^{56} projects into a hydrophobic cavity, while Ile^{52} is exposed to the bulk solvent. Ile^{52} should be involved in hydrophobic interactions with the receptors, since a mutant containing the same mutations as in M3S except for the L29S mutation exhibits an increased receptor binding affinity. The low systemic toxicity of M3S appears to be the effect of the reduced and selective binding affinities for the TNF receptors, and the superior tumor-suppression of M3S appears to be the effect of its weak but longer antitumoral activity *in vivo* compared with wild-type TNF-α. It is also expected that the 1.8-Å resolution structure will serve as an accurate model for explaining the structure-function relationship of wild-type TNF-α and many TNF-α mutants reported previously and for the design of new TNF-α mutants.

TNF-α[1] (cachetin) is a pleiotropic cytokine with a variety of biological activities, including cytotoxicity, immune cell proliferation, and mediation of inflammatory responses (1). It exerts direct cytotoxic effects on a wide range of human and murine tumor cell lines *in vivo* and *in vitro*. TNF-β (lymphotoxin) is a lymphocyte-secreted cytokine with a 32% identity in primary sequence to TNF-α (2). TNF-β exhibits pleiotropic activities similar to those of TNF-α (3, 4). In contrast, the cellular origins, mechanism of induction, and mode of secretion of TNF-α and TNF-β are different, and the two cytokines produce different effects on several lymphoid, endothelial, and other cellular targets (2, 5).

The active form of TNF-α and TNF-β appears to be a homotrimer. The crystal structures of TNF-α and TNF-β revealed that each monomer consists of two antiparallel β-pleated sheets with a jelly roll topology and interacts with each other in a head-to-tail fashion to form a homotrimeric structure (5–7). Diverse activities of TNF are mediated by binding to each of the two receptors, TNF-R55 (55 kDa) and TNF-R75 (75 kDa), on the cell surface. The K_d values of TNF-R55 and TNF-R75 for the two TNFs are approximately 0.5 and 0.1 nM, respectively (4, 8). A number of TNF-α mutants were reported that exhibited altered biological activities and receptor binding affinities (9–14). These mutation studies showed that regions corresponding to the lower part of each cleft between subunits are important for the receptor binding as reviewed previously (14). Indeed, in the crystal structure of TNF-β complexed with TNF-R55, these regions interact with the receptor (15). The TNF and TNF-R55 complex signals a large number of TNF activities, such as cytotoxicity, manganese superoxide dismutase induction, fibroblast proliferation, resistance to chlamidiae synthesis of prostaglandin E_2, and NF-κB induction (16–18), while the TNF and TNF-R75 complex is known to transduce signals for the proliferation of primary thymocytes and T cells (8, 19). In particular, signaling cascades emanating from TNF-R55, which contains death domain, lead cells to apoptosis (6, 8). TNF is also known to exhibit receptor-independent cytotoxic activity by an ion channel formation at acidic pH. Under low pH that disfavors receptor binding, the TNF trimer inserted in the cell membrane resulted in the ion depletion of the cells, most likely through the hole in the middle of the trimeric structure (20–22).

* This work was supported by a G7 grant from KOSEF, by the Basic Science Research Fund from POSTECH, and in part by the Research Center for New Bio-Materials in Agriculture. The costs of publication of this article were defrayed in part by the payment of page charges. This article must therefore be hereby marked "*advertisement*" in accordance with 18 U.S.C. Section 1734 solely to indicate this fact.

The atomic coordinates and structure factors (codes R4TSVSF (for 4TSV) and R4TSWSF (for 4TSW)) have been deposited in the Protein Data Bank, Brookhaven National Laboratory, Upton, NY.

‖ To whom correspondence should be addressed. Tel.: 82-562-279-2289; Fax: 82-562-279-2199; E-mail: bhoh@sb1.postech.ac.kr.

[1] The abbreviations used are: TNF-α, human tumor necrosis factor-α; wtTNF-α, wild type TNF-α; TNF-β, human tumor necrosis factor-β; wtTNF-β, wild type TNF-β; PAGE, polyacrylamide gel electrophoresis.

The clinical use of the potent antitumor activity of TNF-α has been limited by the proinflammatory side effects including fever, dose-limiting hypotension, hepatotoxicity, intravascular thrombosis, and hemorrhage (23–26). Designing clinically applicable TNF-α mutants with low systemic toxicity has been an intense pharmacological interest (1, 23, 27). Human TNF-α, which binds to the murine TNF-R55 but not to the murine TNF-R75, exhibits retained antitumor activity and reduced systemic toxicity in mice compared with murine TNF-α, which binds to both murine TNF receptors (8, 19, 23, 28, 29). Based on these results, many TNF-α mutants that selectively bind to TNF-R55 (L29S, R32W, R32W/S86T, and E146K) have been designed. These mutants displayed cytotoxic activities on tumor cell lines *in vitro* (23, 27, 30, 31), and exhibited lower systemic toxicity *in vivo* (29). Reductions by up to 170-fold were observed for these mutants in TNF-α's priming of human neutrophils for superoxide production and antibody-dependent cell-mediated cytotoxicity, platelet-activating factor synthesis, and adhesion to endothelium (30). In contrast, a human TNF-R75 selective mutant (D143F) did not show lower proinflammatory activities (30), and another TNF-R75-selective double mutant (D143N and A145R) did not exert cytotoxic responses in human KYM-1 cells (27). The hypothesis that the preferential binding of TNF-α to TNF-R55 is related to the low systemic toxicity, however, was disputed in other studies. The R32W and S86T double TNF-α mutant, which binds to TNF-R55 much more preferentially over TNF-R75 developed serious systemic toxicity in a previous experiment in which healthy, anesthetized baboons were infused with the TNF-α double mutant (31). TNF-R55-deficient mice sensitized with D-galactosamine were tolerant of endotoxic shock and insensitive to the TNF toxicities (40–42). Thus, the role of TNF-R55 in the systemic toxicity needs to be investigated further.

Recently, we have found that a human TNF-α mutant containing substitutions of S52I and Y56F, plus a deletion of the N-terminal seven residues, referred to as M3, exhibits increased binding affinities for the two TNF receptors and increased *in vitro* cytotoxicity (32). When the L29S mutation was added, this TNF-α mutant, referred to as M3S hereafter, showed a lower and preferential binding affinity for TNF-R55 and substantially reduced systemic toxicity in mice while inhibiting efficiently the growth of tumors transplanted on mice. M3S displays increased thermal stability, resistance to the trypsin proteolysis, and a longer half-life *in vivo* compared with wtTNF-α. In addition, when combined with paclitaxel, M3S was found to potentiate the antitumor efficacy of paclitaxel through the enhancement of apoptosis (33). Interestingly, the design was recently reported of a TNF-β mutant that exhibits low systemic toxicity but higher antitumor activity than wtTNF-α and wtTNF-β (34). Although the structures of TNF-α mutants are important for understanding their biological activities, the three-dimensional structure of only one TNF-α mutant (A84V) is reported. Here, we report the 1.8- and 2.15-Å crystal structures of M3S in two different crystal packings and discuss the mutational influences on the structure and biological activity of TNF-α.

MATERIALS AND METHODS

Mutant Purification—The *Escherichia coli* host strain used in this study was BL21 (DE3) (F-ompT rB-mB-) whose chromosome carries the T7 RNA polymerase gene under the control of lacUV5 promoter. The gene encoding M3S was inserted downstream of T7 promoter to induce high level expression of the target protein. A double plasmid system including a plasmid for a bacterial chaperone was used to obtain M3S in a soluble form. Construction of these expression vectors and purification schemes was described previously (35).

Cytotoxicity Measurement—The cytotoxic activities of wtTNF-α and M3S were measured on actinomycin D-treated murine L929 cells (ATCC CCL-929) according to the method described previously (36) with slight modification. Briefly, L929 cells were seeded at 1×10^4 cells/well into a 96-well microtiter plate in Dulbecco's modified Eagle's medium containing 2% fetal calf serum. Eighteen hours later, medium containing 2 μg/ml actinomycin D was added to the cell culture together with various concentrations of wtTNF-α or M3S. The cells were incubated for an additional 18 h at 37 °C. Cell viability was determined by measuring the cellular metabolic activity with a 3-[4,5-dimethylthiazol-2-yl]-2,5-diphenyl tetrazolium bromide assay (37).

Systemic Toxicity Measurement—Eight-week-old ICR mice (B & K) with an average body weight of 30 g were used for the systemic toxicity measurement. Several doses of wtTNF-α or M3S were injected intravenously. Lethality was checked 24 h after the single administration, and the systemic toxicity was expressed as LD_{50}, a dose that kills 50% of the mice.

In Vivo Antitumor Activity—A 0.1-ml aliquot of murine MH134 hepatoma cells (1×10^7 cells/ml) was transplanted intradermally into the abdominal wall of 10-week-old female BALB/c mice. In the case of murine Meth A fibrosarcoma, the same amount of tumor cells were injected subcutaneously in the backs of 10-week-old male BALB/c mice. When solid tumors of 3–7 mm in diameter formed, wtTNF-α or M3S was administered intraperitoneally. Control mice received saline in the same schedule for the experimental group. Each group consisted of five mice.

Crystallization and Data Collection—Two different initial crystallization conditions were discovered using the screening method of sparse matrix sampling (38). Refinement of the initial conditions was carried out by using the hanging drop method, and two different crystal forms of M3S were obtained. Crystals of type I (space group R3; $a = b = 66.72$, $c = 85.09$ Å; a monomer in the asymmetric unit) were obtained at 24 °C in the mixture of 2 μl of protein solution (20 mg/ml, in 10 mM HEPES buffer, pH 7.5) and equal volume of 2.8 M sodium formate equilibrated with the same precipitant. Crystals of type II (space group $P2_12_12_1$; $a = 94.17$, $b = 94.56$, $c = 95.89$ Å; two trimers in the asymmetric unit) were obtained in the same way, but using different precipitant solutions containing 25% polyethylene glycol 4000 and 0.1 M sodium citrate buffer, pH 5.6. The crystallization conditions are totally different from those of wild-type and A84V TNF-α mutant in which major precipitants were magnesium sulfate and ammonium sulfate, respectively. The space groups of the two crystals are also different from those of wild-type ($P4_12_12$) (5) and A84V mutant ($P3_121$) TNF-α. All x-ray diffraction data were collected from single crystals with a MacScience DIP2020k imaging plate system mounted on a MacScience M18XHF x-ray generator operated at 50 kV and 90 mA. Data for the type II crystal were collected from a frozen crystal (110 K) soaked in the precipitant solution containing 28% polyethylene glycol 400. All data were processed with the programs DENZO and SCALEPACK.[2] Table I shows relevant data statistics.

TABLE I
X-ray crystallographic data and refinement statistics

	Type I crystal	Type II crystal
Maximum resolution of the data (Å)	1.8	2.15
R_{merge} on I_{hkl} (%)	4.00	7.21
Total number of unique reflections	13102	41282
Completeness of the data (%)	99.0	92.49
Standard *R*-factor (%)	20.0	20.8
Free *R*-factor (%)	26.2	30.7
r.m.s.[a] bond deviation from ideal (Å)	0.015	0.010
r.m.s. angle deviation from ideal (degrees)	2.177	1.992

[a] r.m.s., root mean square.

Structure Determination and Refinement—Structures of M3S were determined using the 2.6-Å structure of wtTNF-α (PDB code 1tnf) (5) by the molecular replacement protocols in the X-PLOR program package (40). A monomeric model and trimeric model were used for the type I and type II crystals, respectively. Peptide segments of residues 19–25, 29–36, 67–73, and 145–150 in each subunit were omitted throughout the molecular replacement procedure, since they contain errors as described in the coordinate description probably due to weak electron densities in these regions. In both cases, strong peaks were observed in the Patterson correlation refinements of the rotation function peaks (41), which were at least 2 times higher than the next highest peaks buried in the noise level. These refined rotation function peaks yielded correct top translation function peaks as judged by the low *R*-factors of

[2] Z. Otwinowski (1996) *The HKL Program Suite*, in preparation.

32.2% for the type I and 34.8% for the type II crystal form (two trimers combined). With the omission of the "problematic regions" mentioned above, a rigid body refinement and an atomic position refinement against reflections at 10–3.0-Å resolution were carried out for each of the translation solutions, resulting in the *R*-factor of 26.5 and 27.0% for the type I and type II crystal form, respectively. Even at this stage, strong electron densities for the two omitted regions, residues 29–36 and 145–150, were observed. Multiple rounds of iterative manual refitting of many main chains and side chains and incorporation of water molecules were carried out according to the $2F_o$-F_c and F_o-F_c electron density maps while gradually increasing the resolution limits to maximums. The current models have reasonable geometry as shown in Table I.

RESULTS AND DISCUSSION

Biological Properties—M3S displays unusual biological properties. The *in vitro* cytotoxicity of M3S is reduced to 5% of wtTNF-α, and the *in vivo* systemic toxicity of M3S, which is indicated by LD_{50}, is 10 times lower than that of wtTNF-α in a lethality test using mice.[3] However, compared with wtTNF-α, a substantial delay in the tumor growth was observed in mice bearing transplanted Meth A fibrosarcoma or MH134 hepatoma solid tumor after M3S was administered intraperitoneally every other day for 10 days.[3] TNF exhibits biological activities mainly through the interactions with the receptors; thereby the distinctive cytotoxic properties of M3S should be directly related to altered interactions with the receptors. M3S exhibits a lower and selective binding affinity for TNF-R55. The affinity for TNF-R55 and TNF-R75 is 11- and 71-fold lower, respectively, compared with wtTNF-α. M3 displayed increased binding affinities for both the receptors by 13- and 11-fold, respectively, and exhibited an increased cytotoxicity.[3] Therefore, in M3S, the I29S mutation counteracts the increased receptor binding affinities by the mutations of S52I and Y56F.

The deletion of up to eight N-terminal amino acids has been known to increase the activity of TNF-α by a factor of 1.5–5, as measured by an L929 cytotoxicity assay (9, 14, 42–44). Our independent assessment of the L929 cytotoxic activity of a mutant lacking the N-terminal seven amino acids showed that the *in vitro* cytotoxicity increased by only about 20% compared with wtTNF-α. Therefore, the deletion minimally affects the cytotoxicities of M3S and M3.

Large Local Conformational Change by the L29S Substitution—The three mutation sites are located at the bottom of the bell-shaped structure of TNF-α as shown in Fig. 1. The structures of M3S reveal the first close-up view of the consequence of L29S mutation in TNF-α, which has been studied extensively due to the preferential binding affinity of the mutant for TNF-R55 (1, 12, 45). While the loop containing residues 29–36, referred as segment A hereafter, is poorly defined in the structure of wtTNF-α, strong electron density of this region was observed for the structures of M3S in the two different crystal packings (Fig. 2, *A* and *B*). The mutation induces the formation of a hydrogen bond between the Ser^{29} OH and the amide nitrogen of Arg^{31}, which is accompanied by many significant changes (Fig. 2*C*). The peptide bonds between Asn^{30} and Arg^{31} and between Ala^{33} and Asn^{34} rotate almost 180° compared with the wtTNF-α and A84V TNF-α mutant. As a result of the peptide bond rotations, the side chain of Asn^{34} moves significantly to form favorable interactions with neighboring residues. These are parts of the intricate interactions of a hydrogen-bonded network involving Asn^{34}, Ala^{35}, four residues from the adjacent subunit (Arg^{82}, Gln^{125}, Glu^{127}, and Asp^{130}), and a cluster of seven water molecules (Fig. 3). The $O^{\delta 1}$ atom of Asn^{34} forms hydrogen bonds with the guanidino group of Arg^{82} in the adjacent subunit and a tightly bound water molecule (*B*-factor = 18.42), which is in a hydrogen bond distance from the amide oxygen of Gln^{125} in the adjacent subunit (Fig. 3). The favorable intra- and intermolecular interactions in M3S, which are not observed in the structure of wtTNF-α or A84V mutant, are consistent with the substantially lower temperature factors of the atoms in segment A than those of wtTNF-α (Fig. 4). Since mutations in segment A are known to affect the biological activities of TNF-α (1, 12, 14, 45), the large local conformational change induced by the L29S mutation as well as the amino acid difference itself should be responsible for the altered binding affinities for the TNF receptors and the *in vivo* activities of the mutant.

FIG. 1. **Ribbon drawing of M3S trimer.** Each subunit is represented by *yellow*, *red*, and *magenta*, respectively. The three mutated residues are in *green ball-and-stick models*. Ser^{29} is located on a loop. Ile^{52} is at the start of a loop, and Phe^{56} is at the beginning of a β-strand.

Superposition of 1.8- and 2.15-Å structures (root mean square deviation of 0.3 Å for backbone atoms) reveals virtually the same conformations of segment A, indicating that the observed conformational change is solely induced by the mutation (Fig. 2, *B* and *C*).

Mutational Effect of S52I and Y56F Substitutions—The conformation of the loop containing mutations, S52I and Y56F, introduced to both M3 and M3S is unambiguously determined. Since Ser^{29} is far apart from these two residues, the conformation of this region would not be affected by the L29S mutation and should be the same in both M3 and M3S. The double mutations do not cause a noticeable conformational change of this loop region. The hydrophobic side chain of Ile^{52} is exposed to the solvent, and Phe^{56} is buried completely in M3S as Ser^{52} and Tyr^{56} are in the structure of wtTNF-α (Fig. 5). Phe^{56} is involved in hydrophobic interactions with Pro^{12}, Val^{41}, Ile^{52}, Leu^{126}, Ile^{154}, and Ala^{156}. Tyr^{56} is an important residue in the interactions between TNF-α and its receptors (5), because several mutants (Y56N, Y56A, and Y56S) displayed impaired or reduced receptor binding and cytotoxic activities (13). The role of Tyr^{56} in the receptor binding, however, has not been satisfactorily explained. Tyr^{56} is not likely to interact with the receptors directly, since the residue is buried completely in the

[3] N.-K. Shin, W. Jeong, H.-C. Shin, manuscript in preparation.

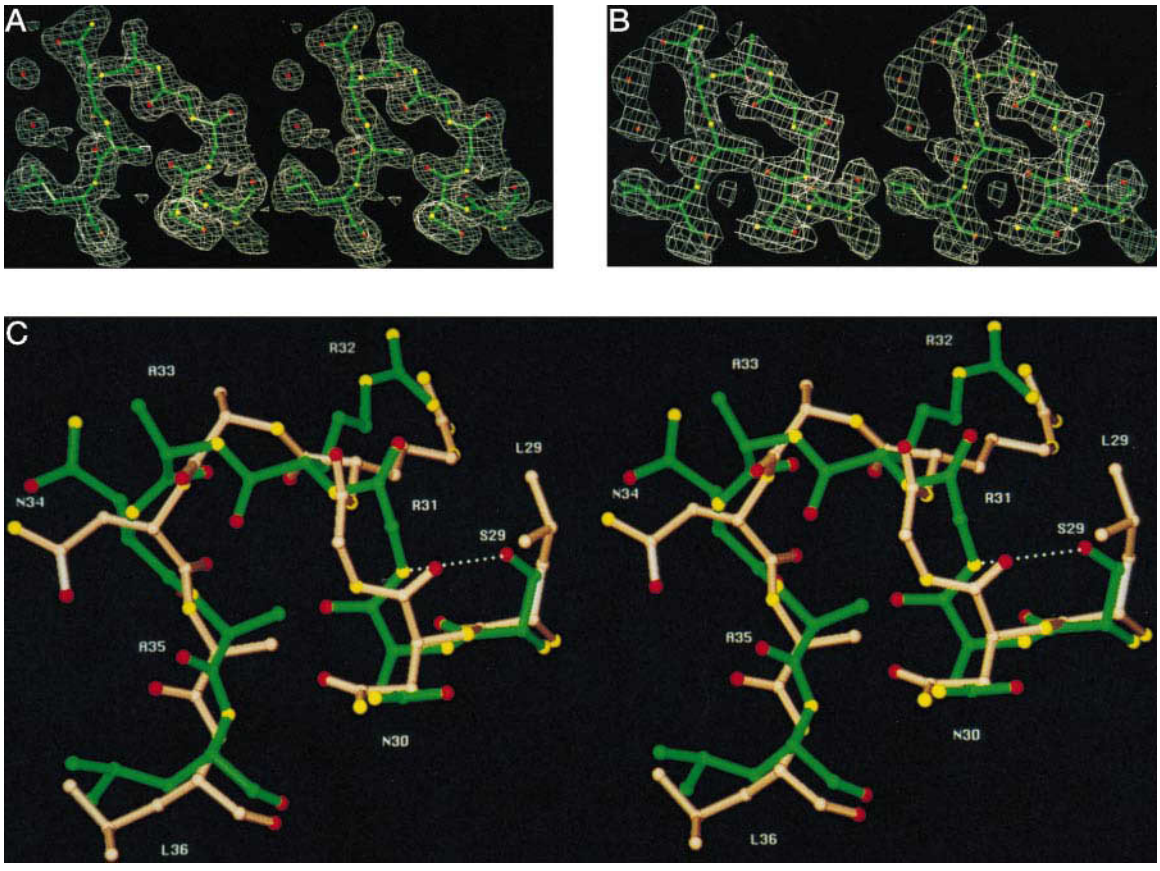

FIG. 2. **Stereo diagrams of segment A (residues 29–36).** *A*, the 1.8-Å $2F_o$-F_c electron density map of the type I crystal. *B*, the 2.15-Å $2F_o$-F_c electron density map of the type II crystal. The maps are contoured at 1.0 σ level. For clarity, the side chains of Arg^{31} and Arg^{32} are omitted. Two water molecules are shown at the same positions in the two different crystal forms. *C*, segment A in the structures of M3S (*green*) and of A84V TNF-α (*tan*). For clarity, the side chain of Arg^{31} is omitted. The *white dotted line* indicates a hydrogen bond. Oxygen and nitrogen atoms are in *red* and *yellow*, respectively. The structure of wtTNF-α was not used because of the coordinate errors in this region. Backbone atoms of residues 8–157 in both structures except for residues 71–72, 84–91, and 105–110 are superimposed.

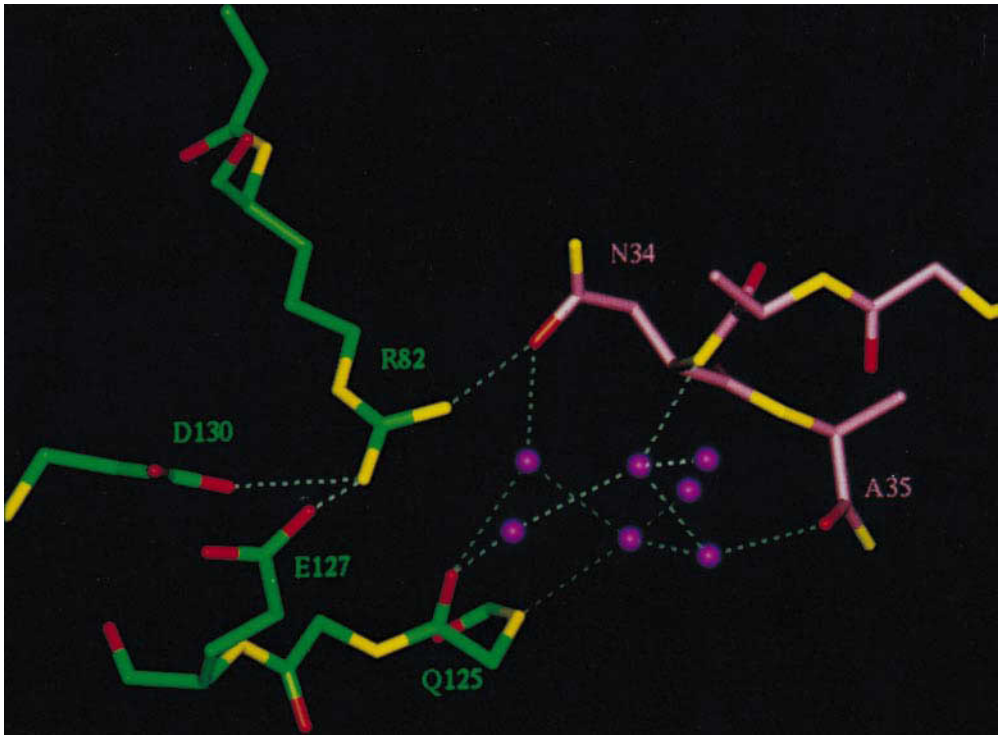

FIG. 3. **A hydrogen-bonded network induced by the I29S mutation.** *White dotted lines* indicate hydrogen bonds. Water molecules are in *magenta*. Oxygen and nitrogen atoms are in *red* and *yellow*, respectively. Each subunit is represented by *green* and *pink*, respectively. Only the side chains involved in the interactions are shown for clarity.

hydrophobic cavity. It was noted that Phe[56] (or Tyr[56] in wtTNF-α) is surrounded by the loop containing residues 50–54, and thus the residue appears important for propping the structure of the loop (Fig. 5). The loop is likely to interact with the receptors directly, since the S52I mutation in M3 increases receptor binding affinity (32). The substitutions of Tyr[56] with a small amino acid, such as Y56A and Y56S, would not support the loop in the proper position for the interaction with the receptor. A similar observation was made in the structure of rat IgG where Phe[27] contacts with the hypervariable loop (residues 31–35) important for interactions with an antigen (46). When phenylalanine was replaced by serine, the affinity of the antibody was reduced drastically because the tight packing of the hypervariable loop was disrupted (47).

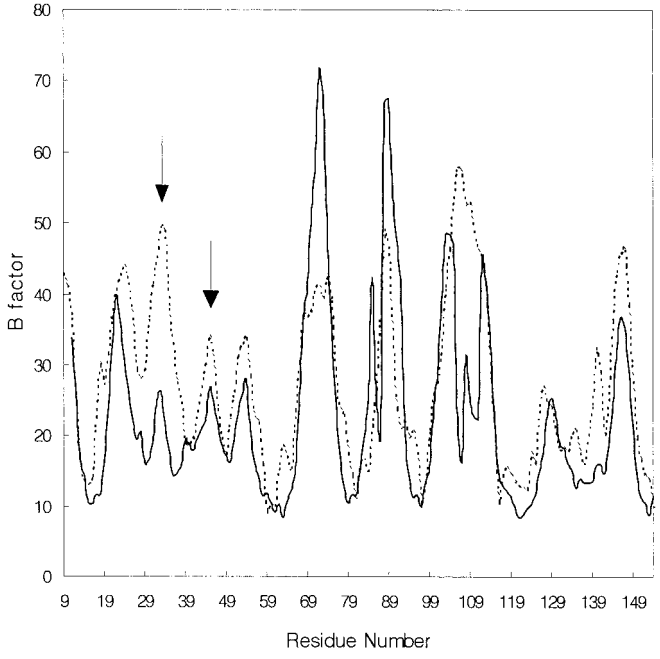

FIG. 4. **The temperature factors of the main chain atoms in the structures of wtTNF-α (*broken line*) and M3S (*solid line*).** *Left* and *right arrows* indicate segment A and the loop containing Arg[44], respectively.

Other Structural Features—The current refined 1.8-Å structure, with coordinate errors less than 0.3 Å, provides much more detailed structural features than the wtTNF-α structure at 2.6 Å and A84V TNF-α mutant structure at 3.0-Å resolution. While the structure of wtTNF-α does not contain any water molecule, a total of 144 water molecules are found in the 1.8-Å structure of M3S trimer, some of which are involved in the intersubunit interactions. Nearly the same disposition of water molecules is found (Fig. 2, *A* and *B*) in the 2.15-Å structure except in the crystal packing interfaces. The backbone atoms of the M3S structure superpose on those of the wtTNF-α structure with the root mean square deviations of 0.66 Å. Relatively large deviations were observed in the loops containing residues 67–73, 84–88, 105–110, 144–150, and segment A, which are poorly defined regions in the wtTNF-α structure. While weak electron densities for residues 67–73, 84–88, and 105–110 were also observed in the structures of M3S in the two different crystal packings, strong electron densities for segment A and residues 144–150 were observed. The two loops are located near the trimer interface, and receptor binding studies suggested that the loop containing residues 144–150 is also involved in the receptor binding (1, 13, 14, 23, 27, 45). Compared with the structure of wtTNF-α, a hydrogen-bonded network is found along this region, which is composed of five tightly bound water molecules, His[15], Ala[146], Ser[147], and two residues belonging to the adjacent subunit (Asn[92] and Leu[93]) (Fig. 6). These extensive interactions should be responsible for the ordered structure of the loop. In the wtTNF-α structure, Arg[32] is involved in a "putative" salt bridge with Glu[146] and a hydrogen bond with Ser[147] (5, 13). In contrast, Arg[32] interacts with the carbonyl oxygen of Phe[144], and Ser[147] interacts directly with Asn[92] of the adjacent subunit in the M3S structure (Figs. 6 and

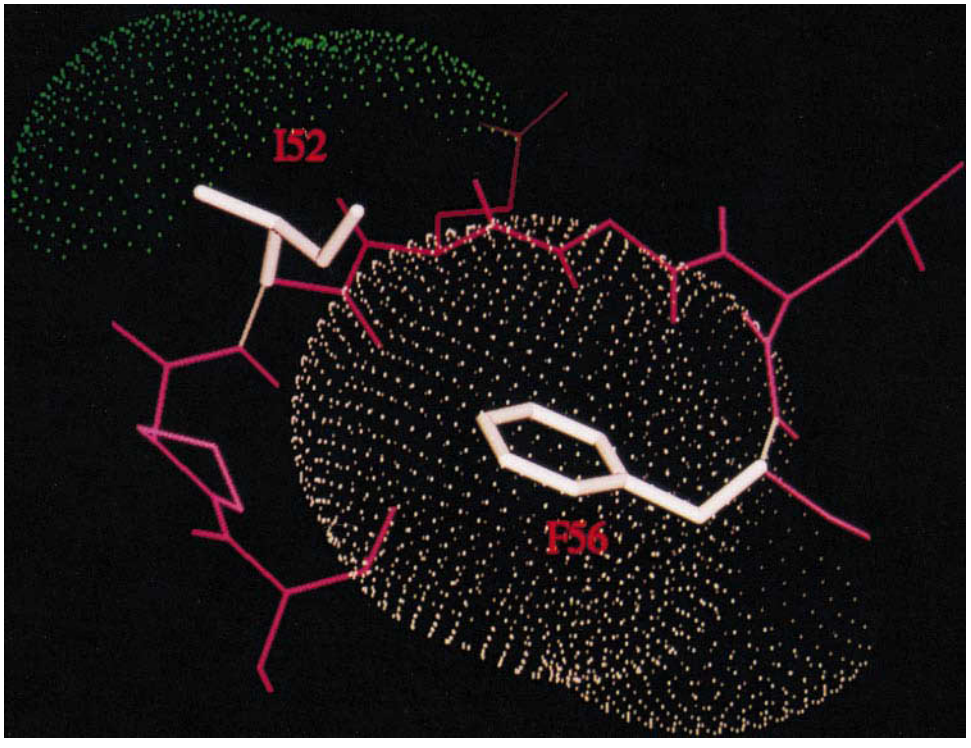

FIG. 5. **The local environment of the loop containing residues 50–56 in M3S.** *Thick white lines* indicate the side chains of Ile[52] and Phe[56]. *Green dots* are the solvent-accessible surface of Ile[52], and *white dots* are the 200% van der Waals radii of the atoms in Phe[56].

7). The peptide bond between Phe^{144} and Ala^{145} is flipped, and the side chain of Phe^{144} is buried more as indicated by the smaller solvent-accessible surface of the residue (33 Å^2) than that of the residue in the wtTNF-α structure (66 Å^2; average value of three subunits) (Fig. 7). In this conformation, the flipped peptide bond orients the carbonyl oxygen of Phe^{144} in the proper position to interact with Arg^{32} via a weakly bound water molecule (*B*-factor = 32.75), and the side chain of Phe^{144} interacts with Ala^{18}, Leu^{142}, Pro^{20}, and Val^{150}, none of which come in contact with Phe^{144} in the structure of wtTNF-α except in one subunit. The one contact between residues 144–150 and segment A via the weakly bound water molecule would hardly be responsible for the local conformational difference of residues 144–150 between wtTNF-α and M3S. Rather, the extensive interactions are also present in the structure of wtTNF-α, and the conformation of the residues 144–150 observed in the M3S structure is the correct conformation.

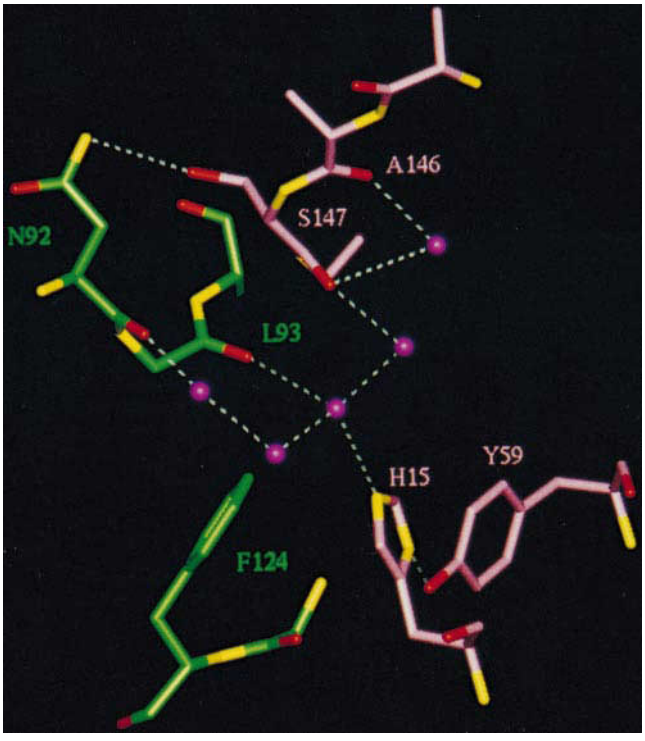

FIG. 6. **Interactions of His^{15} with neighboring residues.** *White dotted lines* indicate hydrogen bonds. Oxygen and nitrogen atoms are in *red* and *yellow*, respectively. Water molecules are in *magenta*. Two adjacent subunits are represented by *green* and *pink*, respectively.

Previously, the analyses of the cytotoxic activities of TNF-α mutants containing a substitution of His^{15} (H15Q, H15N, and H15K) suggested that the residue forms an important hydrogen bond critical for the formation of a bioactive conformer (48). Consistently, the imidazole ring nitrogen of His^{15} interacts with the carbonyl oxygen of Leu^{93} in the adjacent subunit via a water molecule (*B*-factor = 13.06) in the hydrogen-bonded network (Fig. 6). The high resolution structure also shows clearly that the His^{15} is a buried residue (solvent accessibility of 2 Å^2) with its imidazole ring involved in a hydrogen bond with the hydroxyl group of Tyr^{59} and in an aromatic ring stacking with Phe^{124} of the adjacent subunit. These features indicate that His^{15} should be a structurally important residue, and mutations of this residue could result in biologically inactive TNF-α molecules.

Resistance to Proteolysis, Thermal Stability, and Longer Half-life—The limited proteolysis of wtTNF-α by trypsin is known to cleave after Arg^6 and Arg^{44}, while wtTNF-α remained intact following incubation with the SV-8 protease, which recognizes negatively charged amino acids (49). As shown in Fig. 9, M3S is much more resistant to the proteolysis by trypsin compared with wtTNF-α. Superposition of the structures of M3S and wtTNF-α showed that the local environment of the region containing Arg^{44} is nearly identical. Leu^{43} participates in the hydrophobic interaction with Leu^{37}, Val^{16}, Val^{41}, and Leu^{48} (Fig. 8). Asn^{46} is involved in two hydrogen bonds with the carbonyl oxygen of Leu^{26} and the amide nitrogen of Trp^{28}

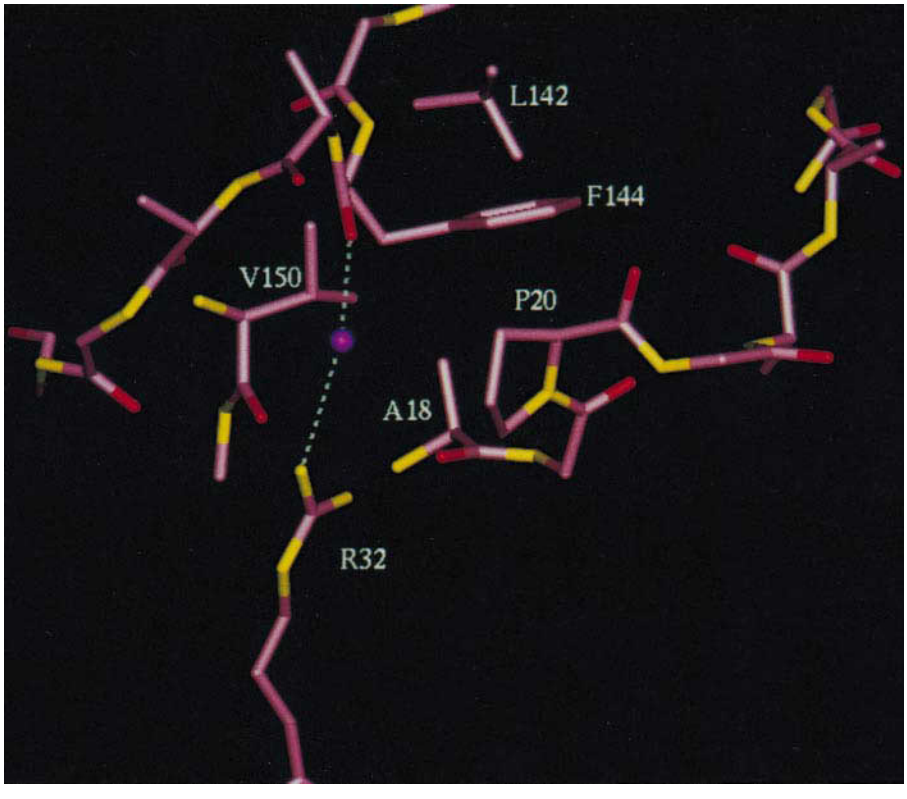

FIG. 7. **Interactions of Phe^{144} and Arg^{32} with neighboring residues.** The *white dotted line* indicates a hydrogen bond. Oxygen and nitrogen atoms are in *red* and *yellow*, respectively. A water molecule is in *magenta*. The side chains except for those involved in the interactions are omitted for clarity.

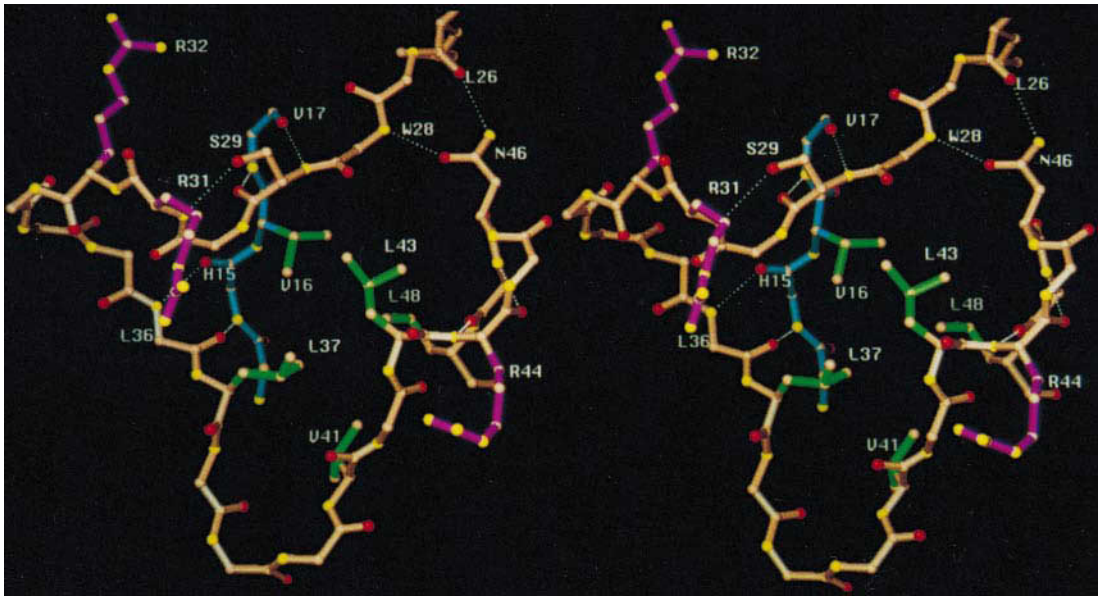

FIG. 8. **Stereo diagram of the interactions of the loop containing Arg^{44} and of the loop containing Arg^{31} and Arg^{32}.** Arginine residues are in *magenta*, and hydrophobic side chains are in *green*. *White dotted lines* indicate hydrogen bonds. Oxygen and nitrogen atoms are in *red* and *yellow*, respectively. Only the side chains involved in the interactions are shown for clarity.

(Fig. 8). These interactions account for lower main chain *B*-factors of residues 43–46 in the structure of both wtTNF-α and M3S compared with other surface-exposed loops (Fig. 4). Thus, it was quite surprising that this rigid loop was reported to be susceptible to trypsin while Arg^{31}-Arg^{32}-Ala^{33} (RRA sequence) on the highly disordered segment A in wtTNF-α was not. However, it was noted that a short fragment, which might be generated from the cleavage after Arg^{31} (or Arg^{32}) and Arg^{44}, could not be detected because the digestion mixture was dialyzed before SDS-PAGE, which identified only the large fragments of residues 7–157 and residues 45–157 along with N-terminal sequencing (49) (Fig. 9). Since the RRA sequence is close to the hydrogen bonds and the hydrophobic interactions involving the loop containing Arg^{44} (Fig. 8), we assumed that the sequence is cleaved first by trypsin, and then the cleavage could result in the disruption of these interactions. As a result, the loop containing Arg^{44} could become flexible and susceptible to trypsin. To confirm this sequential cleavage, we analyzed the peptide fragments generated by trypsin digestion of wtTNF-α using high performance liquid chromatography-mass spectrometry.[4] In the analysis, the peptide fragments corresponding to residues 7–31 (calculated M_r = 2756.1; observed M_r = 2756.5) and residues 33–44 (calculated M_r = 1240.4, observed M_r = 1240.0) were indeed detected. However, the fragments corresponding to residues 7–44 were not detected, supporting the idea that the cleavage at Arg^{31} or Arg^{32} precedes the cleavage at residue 44. The peptide fragments corresponding to residues 33–157 were not detected by either the mass spectrometric analysis or the gel electrophoresis, indicating that the cleavage at residue 44 occurs immediately after the cleavage at Arg^{31} or Arg^{32}. The identification of the major cleavage sites is consistent with the resistance of M3S to trypsin digestion. Since segment A containing the RRA sequence in M3S is rigid compared with wtTNF-α (Fig. 4), the three arginine residues would not be easily accessible to the cleavage by trypsin.

M3S exhibits increased thermal stability and a longer *in vivo* half-life. After incubation at 25 °C for 24 h, 2 times more activity was retained in M3S compared with wtTNF-α in L929 cytotoxicity assay.[3] The *in vivo* half-life of wtTNF-α, which follows a pseudo-zero-order reaction, was 29 min at a dose of 500 μg injected into experimental rats. In comparison, the half-life of M3S was increased to 54 min at a significantly lower dose of 100 μg in the same animal model system. The I29S substitution should confer the thermal stability of M3S, which not only reconstructs segment A into a rigid segment but also increases the intersubunit interactions. Since active trimeric TNF-α slowly converts into inactive monomeric forms (50), the increased thermal stability and resistance to proteolysis of M3S could be the reasons for its longer *in vivo* half-life. It was confirmed that M3 does not show an increased thermal stability.[3]

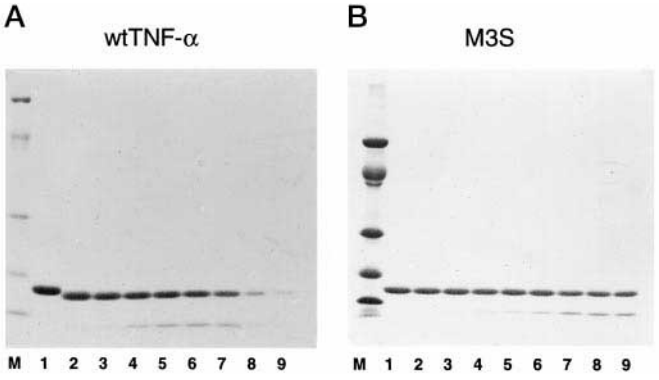

FIG. 9. **SDS-PAGE of 48 h time course trypsin digestion of wtTNF-α and M3S.** The cleaved products are the same bands observed in the early study (49) and correspond to the fragments of residues 7–157 (*upper band*, residues 8–157 in the case of M3S) and residues 45–157 (*lower band*). TNF and trypsin were mixed (100:1, w/w) and incubated at 4 °C for 48 h. A 20-μl aliquot was sampled at each time point and mixed with SDS-PAGE buffer containing 0.125 M Tris-HCl, pH 6.8, 2.15% SDS, 0.005% bromphenol blue, 20% glycerol, and 5% β-mercaptoethanol. The mixture was subjected to SDS-PAGE on 14% polyacrylamide gels. *Lane M* indicates size markers. *Lanes 1–9* indicate the incubation times in hours. *Lane 1*, 0; *lane 2*, 0.5; *lane 3*, 1; *lane 4*, 3; *lane 5*, 5; *lane 6*, 7; *lane 7*, 9; *lane 8*, 24; *lane 9*, 48.

Modulation of Cytotoxicity—The receptor-independent cytotoxicity of TNF mediated by the ion channel-forming activity at low pH (39, 51) requires structural changes. It has been demonstrated that structural plasticity of the TNF-α trimer is a major determinant of its channel-forming activity, and that

[4] Y. J. Kim, S.-S. Cha, J.-S. Kim, N.-K. Shin, W. Jeong, H.-C. Shin, B.-H. Oh, J. H. Hahn, manuscript in preparation.

Gly^{23}, Arg^{32}, and Arg^{44} become highly accessible to proteases Arg-C and V8 after membrane insertion (39). Interestingly, Gly^{23}, Trp^{28}, Arg^{32}, and Arg^{44} are on or near segment A, implying that the flexible structure of segment A in wtTNF-α may play a key role in the ion channel formation. Thus, M3S is not likely to undergo structural changes essential for the ion channel formation as easily as wtTNF-α due to the rigidity of segment A. It is possible that the increased stability of M3S could result in a lower receptor-independent cytotoxicity.

Taken together, the desirable low systemic toxicity of M3S is likely to be the effect of the reduced binding affinities for the two TNF receptors with the preferential binding affinity for TNF-R55, and possibly of a reduced receptor-independent cytotoxicity *in vivo*. The superior tumor-suppressing activity of M3S, despite its lower cytotoxicity, is likely to be the result of the extended antitumoral activity due to its longer *in vivo* half-life. The concept of attenuated but prolonged biological effects of TNF-α *in vivo* may be a key for designing therapeutically valuable TNF molecules.

In summary, the comparison of the crystal structures of M3S and wtTNF-α reveals that 1) the L29S mutation results in favorable intra- and intersubunit interactions, which should be responsible for the increased thermal stability, resistance to proteolytic cleavage, and altered receptor binding affinities; 2) the I52S and Y56F mutations do not induce a noticeable conformational change; 3) substituted Ile^{52} is exposed to the bulk solvent and is likely to interact with the TNF receptors favorably as it is supported by the increased binding affinities of M3 for the receptors. The structural analyses of M3S structures led to the identification of the major proteolytic cleavage sites at Arg^{31}-Arg^{32}-Ala^{33} by a mass spectrometric method. The analyses also provided structural bases for the previous conclusions that His^{15} and Tyr^{56} are important for the bioactive conformation and/or the receptor binding. It is also anticipated that the high resolution structure of M3S will serve as a better model to explain the structure-function relationship of wtTNF-α and many other TNF-α mutants generated so far and for the design of other TNF-α mutants with therapeutic potentials.

Acknowledgment—This study made use of the x-ray facility at Pohang Light Source.

REFERENCES

1. Van Ostade, X., Vandenabeele, P., Tavernier, J., and Fiers, W. (1994) *Eur. J. Biochem.* **220,** 771–779
2. Eck, M. J., Ultsch, M., Rinderknecht, E., de Vos, A. M., and Sprang, S. R. (1992) *J. Biol. Chem.* **267,** 2119–2122
3. Aggarwal, B. B., Eessalu, T. E., and Hass, P. E. (1985) *Nature* **318,** 665–667
4. Smith, C. A., Davis, T., Anderson, D., Solam, L., Beckmann, M. P., Jerzy, R., Dower, S. K., Cosman, D., and Goodwin, R. G. (1990) *Science* **248,** 1019–1023
5. Eck, M. J., and Sprang, S. R. (1989) *J. Biol. Chem.* **264,** 17595–17605
6. Itoh, N., and Nagata, S. (1993) *J. Biol. Chem.* **268,** 10932–10937
7. Beutler, B., and Cerami, A. (1988) *Annu. Rev. Biochem.* **57,** 505–518
8. Tartaglia, L. A., and Goeddel, D. V. (1992) *Immunol. Today* **13,** 151–153
9. Creasey, A. A., Doyle, L. V., Reynolds, M. T., Jung, T., Lin, L. S., and Vitt, C. R. (1987) *Cancer Res.* **47,** 145–149
10. Nakamura, S., Kata, A., Masegi, T., Fukuoka, M., Kitai, K., Ogawa, H., Ichikawa, Y., Maeda, M., Watanabe, N., and Niitsu, Y. (1991) *Int. J. Cancer* **48,** 744–748
11. Masegi, T., Nakamura, S., Fukuoka, M., Kitai, K., Ichikawa, Y., Watanabe, N., and Niitsu, Y. (1993) *Biotechnol. Lett.* **15,** 1107–1110
12. Van Ostade, X., Tavernier, J., Prange, T., and Fiers, W. (1991) *EMBO J.* **10,** 827–836
13. Zhang, X.-M., Weber, I., and Chen, M.-J. (1992) *J. Biol. Chem.* **267,** 24069–24075
14. Van Ostade, X., Tavernier, J., and Fiers, W. (1994) *Protein Eng.* **7,** 5–22
15. Banner, D. W., D'Aracy, A., Janes, W., Gentz, R., Schoenfeld, H.-J., Broger, C., Loetscher, H., and Lesslauer, W. (1993) *Cell* **73,** 431–445
16. Engelmann, H., Holtmann, H., Brakebusch, C., Avni, Y. S., Sarov, I., Nophar, Y., Hadas, E., Leitner, O., and Wallach, D. (1990) *J. Biol. Chem.* **265,** 14497–14504
17. Espevik, T., Brockhaus, M., Loetscher, H., Norstad, U., and Schalaby, M. R. (1990) *J. Exp. Med.* **171,** 415–426
18. Schalaby, M. R., Sundan, A., Loetscher, H., Brockhaus, M., Lesslauer, W., and Espevik, T. (1990) *J. Exp. Med.* **172,** 1517–1520
19. Tartaglia, L. A., Weber, R. F., Figari, I. S., Reynolds, C., Palladino, M. A. J., and Goeddel, D. V. (1991) *Proc. Natl. Acad. Sci. U. S. A.* **88,** 9292–9296
20. Baldwin, R. L., Chang, M. P., Bramhall, J., Gravas, S., Bonavida, B., and Wisnieski, B. J. (1988) *J. Immunol.* **141,** 2352–2357
21. Chang, M. P., and Wisnieski, B. J. (1990) *Infect. Immun.* **58,** 2644–2650
22. Baldwin, R. L., Mirzabekov, T., Kagan, B. L., and Wisnieski, B. J. (1995) *J. Immunol.* **154,** 790–798
23. Van Ostade, X., Vandenabeele, P., Everaerdt, B., Loetscher, H., Gentz, R., Brockhaus, M., Lesslauer, W., Tavernier, J., Brouckaert, P., and Fiers, W. (1993) *Nature* **361,** 266–269
24. Hauser, G. J., McIntosh, J. K., Travis, W. D., and Rosenberg, S. A. (1990) *Cancer Res.* **50,** 3503–3508
25. Kilbourn, R. G., Gross, S. S., Jubran, A., Adams, J., Griffith, O. W., Levi, R., and Lodato, R. F. (1990) *Proc. Natl. Acad. Sci. U. S. A.* **87,** 3629–3632
26. Van Der Poll, T., Van Deventer, S. J. H., Hack, C. E., Wolbink, G. J., Avarden, L. A., Buller, H. R., and Ten Cate, J. W. (1992) *Blood* **79,** 693–698
27. Loetscher, H., Stueber, D., Banner, D., Mackay, F., and Lesslauer, W. (1993) *J. Biol. Chem.* **268,** 26350–26357
28. Loetscher, H., Steinmetz, M., and Lesslauer, W. (1991) *Cancer Cells* **3,** 221–226
29. Brockhaus, M., Schoenfeld, H.-J., Schlaeger, E.-J., Hunziker, W., Lesslauer, W., and Loetscher, H. (1990) *Proc. Natl. Acad. Sci. U. S. A.* **87,** 3127–3131
30. Babara, J. A. J., Smith, W. B., Gamble, J. R., Van Ostade, X., Vandenabeele, P., Tavernier, J., Fiers, W., Vadas, M. A., and Lopez, A. F. (1994) *EMBO J.* **13,** 843–850
31. Van Zee, K. J., Stackpole, S. A., Montegut, W. J., Rogy, M. A., Calvano, S. E., Hsu, K. C., Chao, M., Meschter, C. L., Loetscher, H., Stuber, D., Ettlin, V., Wipf, B., Lesslauer, W., Lowry, S. F., and Moldawer, L. L. (1994) *J. Exp. Med.* **179,** 1185–1191
32. Shin, N.-K., Lee, I., Jang, S.-G., and Shin, H.-C. (1994) *Proc. BPERC Int. Symp.* **94,** 43–50
33. Seong, J., Milross, C. G., Hunter, N. R., Shin, H. C., and Milas, L. (1997) *Anti-Cancer Drugs* **8,** 80–87
34. Taniyama, M., Morita, T., Yamagishi, Y., Kato, A., Bando, C., Okawa, N., and Kaji, A. (1997) *Proc. Natl. Acad. Sci. U. S. A.* **94,** 3324–3329
35. Jeong, W., Shin, N.-K., and Shin, H.-C. (1997) *Biotechnol. Lett.* **19,** 579–582
36. Ruff, M. R., and Gifford, G. E. (1980) *J. Immunol.* **125,** 1671–1677
37. Mosmann, T. (1983) *J. Immunol. Methods* **65,** 55–63
38. Jancarik, Y., and Kim, S.-H. (1991) *J. Appl. Crystallogr.* **24,** 409–411
39. Baldwin, R. L., Stolowitz, M. L., Hood, L., and Wisnieski, B. J. (1996) *Proc. Natl. Acad. Sci. U. S. A.* **93,** 1021–1026
40. Brünger, A. T. (1992) *X-PLOR (Version 3.0) Manual*, Yale University, New Haven, CT
41. Brünger, A. T. (1990) *Acta Crystallogr. Sec. A* **46,** 46–57
42. Geigert, J., Panschar, B. M., Taforo, C., Paola, J., Fong, S., Huston, H. N., Wong, D. E., and Wong, D. Y. (1987) *Dev. Biol. Stand.* **69,** 129–138
43. Tsujimoto, M., Tanaka, S., Sakuragawa, Y., Tsuruoka, N., Funakoshi, K., Butsugan, T., Nakazato, H., Nishihara, T., Nogushi, T., and Vilcek, J. (1987) *J. Biochem.* **101,** 919–925
44. Sidhu, R. S., and Bollon, A. P. (1989) *Anticancer Res.* **9,** 1569–1576
45. Yamagishi, J., Kawashima, H., Matsuo, N., Ohue, M., Yamayoshi, M., Fukui, T., Kotani, H., Furuta, R., Nakano, K., and Yamada, M. (1990) *Protein Eng.* **3,** 713–719
46. Marquart, M., Deisenhofer, J., Huber, R., and Palm, W. (1980) *J. Mol. Biol.* **141,** 369–391
47. Riechmann, L., Clark, M., Waldmann, H., and Winter, G. (1988) *Nature* **332,** 323–327
48. Yamamoto, R., Wang, A., Vitt, C. R., and Lin, L. S. (1989) *Protein Eng.* **2,** 553–558
49. Narhi, L. O., Rhode, M. F., Hunt, P., and Arakawa, T. (1989) *J. Protein Chem.* **8,** 669–677
50. Schuchmann, M., Hess, S., Bufler, P., Brakebusch, C., Wallach, D., Porter, A., Riethmuller, G., and Engelmann, H. (1995) *Eur. J. Immunol* **25,** 2183–2189
51. Kagan, B. L., Baldwin, R. L., Munoz, D., and Wisnieski, B. J. (1992) *Science* **255,** 1427–1430